Sensors and Materials, Vol. 36, No. 5 (2024) 1825–1834 1825
MYU Tokyo

S & M 3637

Fabrication and Measurement of Cosputtered Indium Gallium Oxide Ultraviolet Photodetectors

Artde Donald Kin-Tak Lam,[1] En-Min Huang,[2]
Sheng-Po Chang,[3*] and Shoou-Jinn Chang[2]

[1]School of Design & Straits College of Engineering, Fujian University of Technology,
No. 3 Xueyuan Road, University Town, Fuzhou City, Fujian Province, China
[2]Institute of Microelectronics & Department of Electrical Engineering, National Cheng Kung University,
Tainan City 70101, Taiwan
[3]Department of Microelectronics Engineering, National Kaohsiung University of Science and Technology,
Kaohsiung City 811, Taiwan

(Received September 4, 2023; accepted April 10, 2024)

Keywords: indium gallium oxide, ultraviolet photodetector, cosputtering, responsivity, response time

Indium gallium oxide (IGO) ultraviolet (UV) photodetectors (PDs) were fabricated by cosputtering. The power of the gallium oxide target was fixed at 80 W, while the power of the indium oxide target was varied at 20, 30, 40, and 80 W. As the amount of indium doping increased, the dark current and response decay time increased. Furthermore, the sensitivity and responsivity of the PDs also increased, reaching the maximum values of 5.20×10^3 at 30 W/80 W and 1.72×10^2 A/W at 40 W/80 W, respectively. However, excessive indium doping resulted in excessively high dark current and increased sensitivity and response decay time. Therefore, proper control of indium doping can lead to high-performance IGO UV PDs.

1. Introduction

Ultraviolet (UV) photodetectors (PDs) have received much attention in the past decade owing to the increase in UV radiation. UV radiation is a form of electromagnetic radiation with wavelengths shorter than those of visible light but longer than X-rays. The UV spectrum is typically divided into three regions,(1) UV-A, UV-B, and UV-C. UV-A (315–400 nm) has the longest wavelength among the three UV regions and is closest to visible light. UV-B (280–315 nm) radiation has a higher energy than UV-A, which means it can cause more severe damage to the skin, causing skin swelling and extreme pain. However, it is blocked by the ozone layer, so only a small amount reaches the earth's surface.(2) At wavelengths below 200 nm, vacuum UV rays can be absorbed by air. Therefore, the wavelength of UV-C that can pass through the atmosphere is between 200 and 280 nm. The shorter the wavelength, the more dangerous it is, but because the ozone layer can completely block UV-C, all living things on earth will be protected from UV-C. UV PDs find utility in a wide range of commercial and military applications.(3–5) They can be divided into two categories in accordance with wavelength:

*Corresponding author: e-mail: changsp@nkust.edu.tw
https://doi.org/10.18494/SAM4801

ISSN 0914-4935 © MYU K.K.
https://myukk.org/

visible-blind PDs (280 < $\lambda \leq$ 400 nm) and solar-blind PDs ($\lambda \leq$ 280 nm). With visible-blind PDs, we can detect the outdoor UV intensities of UV-A (315–400 nm) and UV-B (280–315 nm) radiation. Solar-blind PDs detect UV radiation but are insensitive to the longer wavelengths of visible and infrared light. They can also be used to detect flame and UV signatures in military applications.[6] The most important thing for humans is that long exposure to UV light can cause sun damage to the surface skin, DNA damage and mutation, and also eye damage. Hence, the development of UV PDs exhibiting superior sensitivity and exceptional selectivity is crucial. As technology advances, PDs achieve better response and miniaturization. There are numerous approaches to achieving better performance of the PD, such as modifying its structures or developing new sensing materials. Among all the different types of PD structure, we chose metal–semiconductor–metal (MSM) as our study structure.[7–10] It consists of two metal contacts (electrodes) placed on a semiconductor material, creating a sandwich-like structure. It offers advantages such as high-speed response, high sensitivity, and compatibility with integrated circuit fabrication processes. As the sensing materials, we chose metal oxide semiconductor-based sensors because of their low cost, high efficiency, and easy fabrication. Ga_2O_3 is a potential material for electronic applications because of its wide bandgap, high electron mobility, UV transmittance, and physical and chemical stability.[11,12] However, it has the fatal flaw of low conductivity, which limits its development. Fortunately, we can improve the conductivity by doping it with other materials, such as SnO_2, ZnO, and In_2O_3.[13] In this study, we deposited In/Ga oxide thin film as our active layer material by cosputtering to achieve a high-performance sensor. Ga_2O_3 is an n-type material with a wide bandgap (around 4.8–5.3 eV) and demonstrates excellent transmittance in the deep-UV region, making it suitable for UV optoelectronic devices such as UV PDs, sensors, and LEDs. Also, it exhibits good physical and chemical stability, ensuring its reliability and longevity under high-temperature operating conditions.[14,15] In_2O_3 is also an n-type material with a wide bandgap (around 2.8–3.3 eV), and it exhibits both high electrical conductivity and high optical transparency.[16,17] By mixing Ga_2O_3 and In_2O_3, indium gallium oxide (IGO) with the bandgap of 4.2–4.6 eV is formed, which combines the advantages of Ga_2O_3 and In_2O_3, improving the demerit of the low conductivity of Ga_2O_3. Gallium and indium, both belonging to Group 13, exhibit stable oxidation states of +3 in their respective oxides.[18] The similarity in chemistry makes IGO a promising material, and we chose it as the active layer in this study.[19–22]

2. Experimental Procedure

The fabricated devices consist of a quartz substrate, IGO thin film deposited by cosputtering, and Ni/Au interdigitated electrodes. Before the fabrication, the 2 cm × 2 cm quartz substrate was cleaned by soaking in acetone, isopropanol, and deionized (DI) water in sequence and vibrated in a ultrasonic bath for five minutes. Finally, it was dried with a nitrogen gun. After cleaning the substrate, a radio frequency (RF) magnetron sputter system was used to deposit the IGO thin film (150 nm) as the active layer at room temperature. In this study, cosputtering with the two targets of In_2O_3 and Ga_2O_3 is introduced. The RF power of the Ga_2O_3 target was fixed at 80 W, whereas the RF power of the In_2O_3 target was varied as 20, 30, 40, and 80 W with the chamber

pressure of 5 mTorr. In the last step, Ni/Au (30 nm/70 nm) electrodes with width/length (W/L) of 0.1 mm/1.2 mm and the finger distance of 0.2 mm were deposited through a mask using electron beam (E-beam) evaporation equipment. Atomic force microscopy (AFM) was used to observe the surface morphology and roughness of the film. Energy-dispersive X-ray spectroscopy (EDS) was used to determine the ratio of element composition. An Agilent B1500A semiconductor parameter analyzer was used to measure the current–voltage (*I*–*V*) characteristics of the devices.

3. Results and Discussion

The surface morphology and roughness of the film were measured by AFM. As shown in Fig. 1, the cosputtered films were investigated, varying the RF sputtering power of the In_2O_3 target as 20, 30, 40, and 80 W, while keeping the power of the Ga_2O_3 target at 80 W. Table 1 shows the average root mean square (RMS) surface roughness values of IGO films. Lower values represent smoother surfaces.[23] Therefore, the measurement results indicate that the surface roughness of the cosputtered films is lower than that of pure indium oxide [Fig. 1(a)].

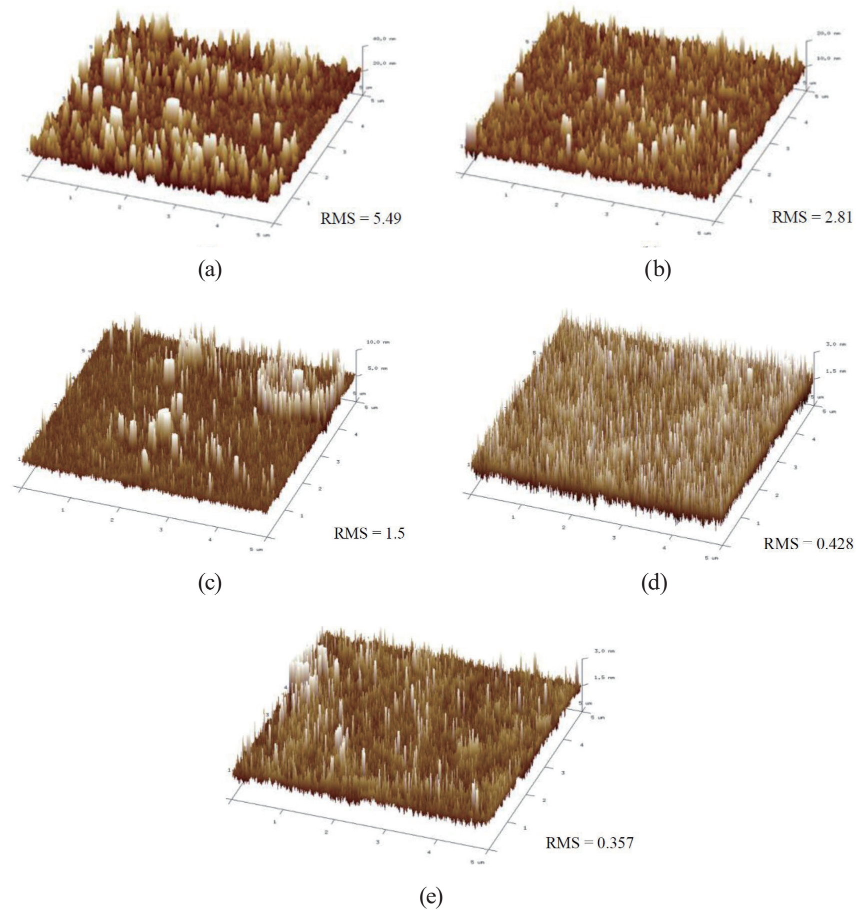

Fig. 1. (Color online) AFM images of surface roughnesses of cosputtering film. (a) Pure In_2O_3, (b) 20 W/80 W, (c) 30 W/80 W, (d) 40 W/80 W, and (e) 80 W/80 W.

Table 1
Average RMS surface roughness values of IGO films.

In_2O_3/Ga_2O_3	Average RMS (nm)
80 W/0 W	5.49
20 W/80 W	2.81
30 W/80 W	1.5
40 W/80 W	0.428
80 W/80 W	0.357

The ratio of element composition was determined by EDS analysis. Figure 2 shows the EDS spectrum and the atomic ratio of the thin film. The In/Ga ratios with In_2O_3 target powers of 20, 30, 40, and 80 W were 25.1, 44.7, 69.8, and 136%, respectively. We can observe that when the In_2O_3 target power increases, the ratio of indium to gallium also increases, which means that the proportion of indium increases, and the conductivity will improve.

Figure 3 shows the Tauc plots and linear fitting of absorption spectra. We apply the Tauc relation to calculate the energy bandgap.(24,25)

$$(\alpha hv)^2 = (hv - E_g) \tag{1}$$

Here, α represents the absorption coefficient, hv is the photoenergy, and E_g is the energy bandgap.

In Fig. 3, the bandgaps of 20 W/80 W, 30 W/80 W, and 40 W/80 W thin films are seen to be 4.6, 4.3, and 4.2 eV, respectively. As a result, the more indium is doped, the smaller the energy band.

The *I–V* characteristics of the fabricated IGO PDs are shown in Fig. 4. The dark current of the 80 W/80 W film is too large to measure (exceeding 100 mA); that of the 40 W/80 W film is also large but still within the measurement range. However, only the photocurrent in the maximum response wavelength (320 nm) was measured. For the 20 W/80 W and 30 W/80 W films, both dark current and photocurrent with incident illumination of 220 to 500 nm were measured. Under 10 V applied bias, the measured photocurrents were 2.44×10^{-10}, 1.46×10^{-6}, and 4.25×10^{-2} A, and the dark currents were 2.69×10^{-12}, 2.8×10^{-10}, and 2.64×10^{-2} A for the 20 W/80 W, 30 W/80 W, and 40 W/80 W films, respectively. Therefore, it is understood that when the proportion of doped indium increases, the current also increases owing to the good conductivity of In_2O_3. Furthermore, the photo/dark current ratios were 91.5, 5.20×10^3, and 1.61 for the 20 W/80 W, 30 W/80 W, and 40 W/80 W films, respectively, which indicated that the 30 W/80 W film has a high photo/dark current ratio that is suitable for light sensing, and the low photo/dark current ratio of the 40 W/80 W film is due to its high current value.

Responsivity is the ability of PDs to convert incident light into photoelectrons and can be expressed as follows.

$$R = \frac{I_{photo} - I_{dark}}{P_{in}} \tag{2}$$

I_{photo} is the photocurrent, I_{dark} is the dark current, and P_{in} is the power of incident light.

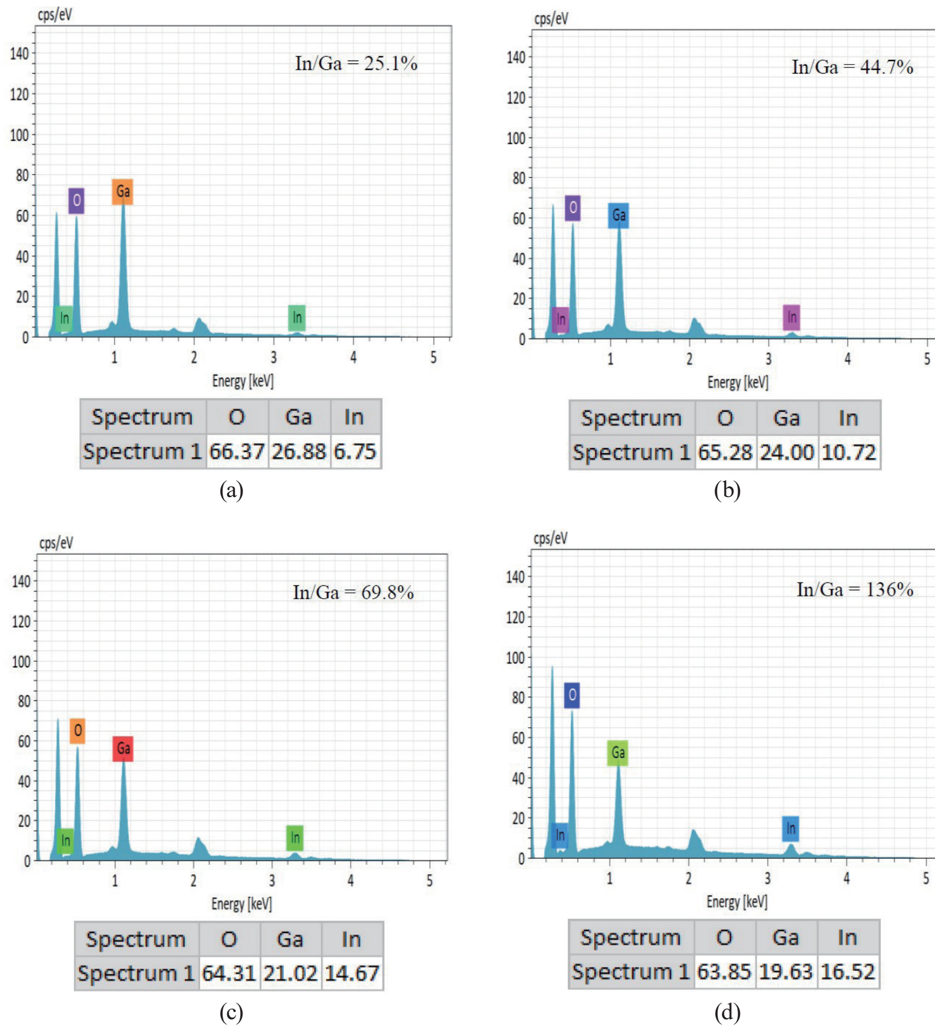

(a)

Spectrum	O	Ga	In
Spectrum 1	66.37	26.88	6.75

(b)

Spectrum	O	Ga	In
Spectrum 1	65.28	24.00	10.72

(c)

Spectrum	O	Ga	In
Spectrum 1	64.31	21.02	14.67

(d)

Spectrum	O	Ga	In
Spectrum 1	63.85	19.63	16.52

Fig. 2. (Color online) Results of EDS analysis of cosputtered film: (a) 20 W/80 W, (b) 30 W/80 W, (c) 40 W/80 W, and (d) 80 W/80 W.

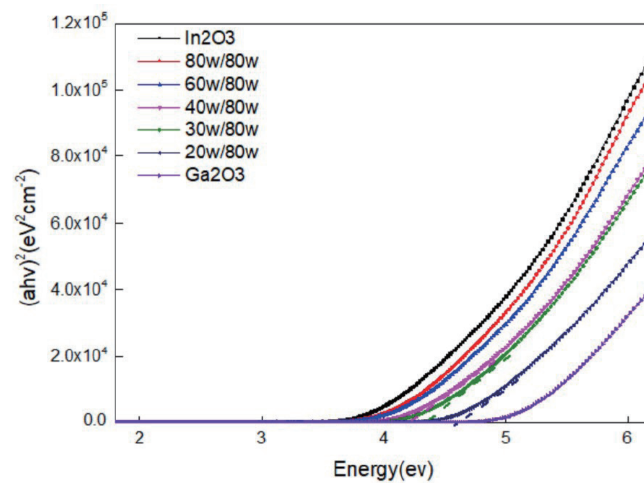

Fig. 3. (Color online) Tauc plots and linear fitting of the absorption spectra of the as-deposited IGO thin films.

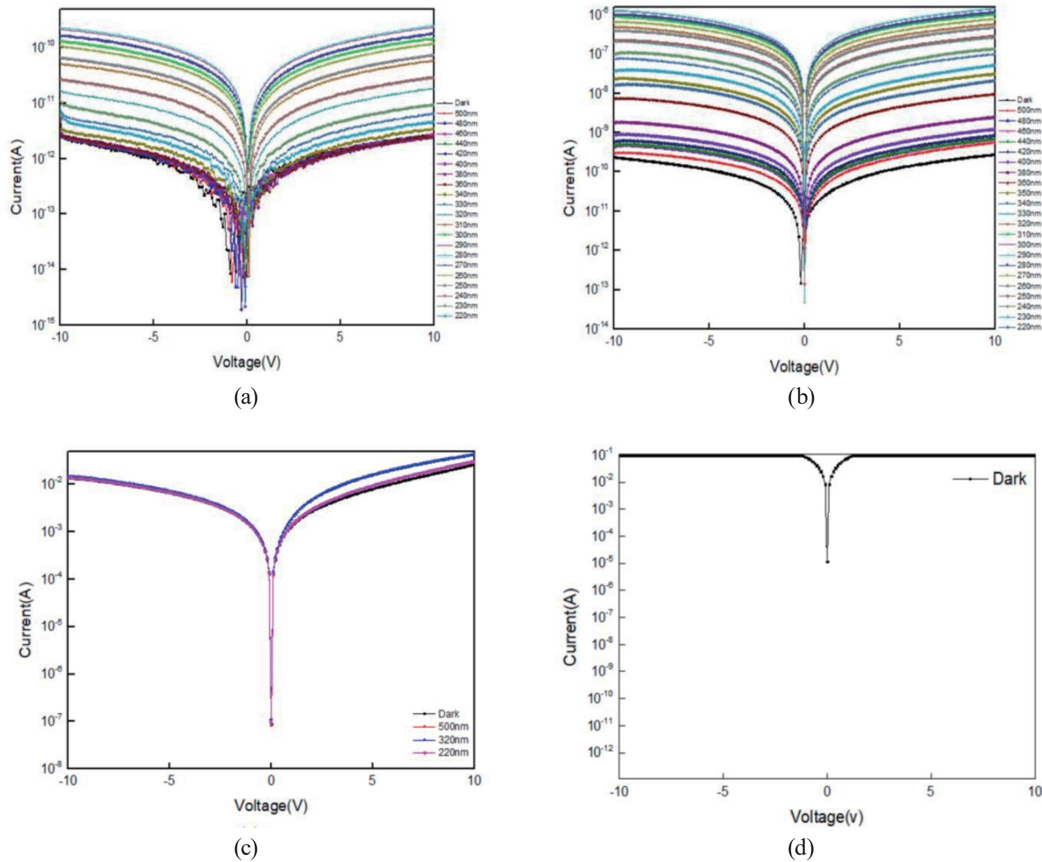

Fig. 4. (Color online) *I–V* characteristic of IGO PDs: (a) 20 W/80 W, (b) 30 W/80 W, (c) 40 W/80 W, and (d) 80 W/80 W.

The responsivities of the 20 W/80 W, 30 W/80 W, and 40 W/80 W films were 4.66×10^{-6}, 2.21×10^{-2}, and 1.72×10^{2} A/W, respectively, indicating that when the ratio of indium doping increases, the responsivity also increases. It indicates that when the doped indium content increases, the responsivity will increase. Under UV illumination, the oxygen-related states could generate more photocarriers, increasing the responsivity.[26] Figure 5 shows the dynamic response of the devices. We chose a specific wavelength for each sample which devices under illumination with the highest photocurrent. Five cycles of dynamic optical response with the wavelength for each sample were 280, 290, and 320 nm for the 20 W/80 W, 30 W/80 W, and 40 W/80 W films, respectively. The process of turning on and off is included in each cycle. The detectors were turned on by illuminating for 3 min (20 W/80 W), 5 min (30 W/80 W), and 2 min (40 W/80 W), then turned off by covering the light source for 2 min (20 W/80 W), 3 min (30 W/80 W), and 2 min (40 W/80 W). Rise and decay times are also important parameters of PDs. Therefore, the rise time (from 0 to 90%) and decay time (from 90 to 0%) were investigated. The results are summarized in Table 2. When more indium is doped, the rise/decay times are longer because it takes more time to generate more photocarriers.[27,28] However, when doping continues to increase, the dark current increases so that it saturates relatively quickly, thus shortening the rise/decay times.

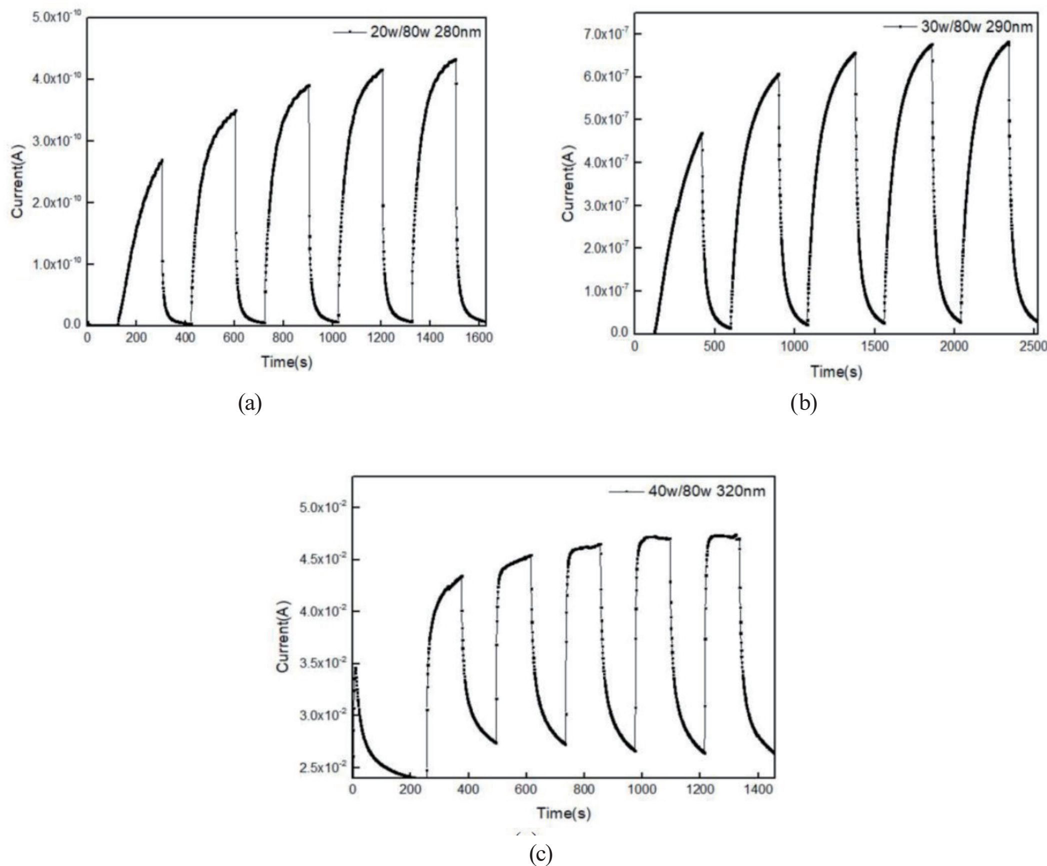

(a) (b)

(c)

Fig. 5. Dynamic responses of (a) 20 W/80 W, (b) 30 W/80 W, and (c) 40 W/80 W films.

Table 2
Rise/decay times of IGO PDs.

In/Ga oxide	Rise time (s)	Decay time (s)
20 W/80 W	250	27
30 W/80 W	465	103
40 W/80 W	7	60

4. Conclusions

In this study, a series of MSM UV PDs with different cosputtering conditions were fabricated in an RF sputter system and with E-beam evaporation. Doping In_2O_3 into Ga_2O_3 can improve the dark current and optical properties, but excess doping might limit the applications of PDs because of excessive dark current. The sensitivity showed the highest value of 5.2×10^3 for the 30 W/80 W film and the responsivity showed the largest value of 1.72×10^2 (A/W) for the 40 W/80 W film. Finally, the 40 W/80 W film had the shortest rise time of 7 s and the 20 W/80 W film had the shortest decay time of 27 s. Therefore, proper control of indium doping can lead to high-performance IGO UV PDs.

Acknowledgments

The authors would like to thank the National Science and Technology Council, Taiwan, for financially supporting this research under Contract Nos. NSTC 112-2221-E-006-117-MY3 and 112-2218-E-006-010-MBK. The authors gratefully acknowledge the Instrument Center of National Cheng Kung University for allowing the use of JEOL JEM-2100F CS STEM equipment.

References

1 B. L. Diffey: Methods **28** (2002) 4. https://doi.org/10.1016/S1046-2023(02)00204-9
2 X. Guo, N. Hao, D. Guo, Z. Wu, Y. An, X. Chu, L. Li, P. Li, M. Lei, and W. Tang: J. Alloys Compd. **660** (2016) 136. https://doi.org/10.1016/j.jallcom.2015.11.145
3 G. Hu, C. Shan, N. Zhang, M. Jiang, S. Wang, and D. Shen: Opt. Express **23** (2015) 13554. https://doi.org/10.1364/OE.23.013554
4 D. Jiang, L. Li, H. Chen, H. Gao, Q. Qiao, Z. Xu, and S. Jiao: Appl. Phys. Lett. **106** (2015) 171103. https://doi.org/10.1063/1.4918991
5 H. Shen, C. Shan, B. Li, B. Xuan, and D. Shen: Appl. Phys. Lett. **103** (2013) 232112. https://doi.org/10.1063/1.4839495
6 Q. Wang, J. Chen, P. Huang, M. Li, Y. Lu, K. P. Homewood, G. Chang, H. Chen, and Y. He: Appl. Surf. Sci. **489** (2019) 101. https://doi.org/10.1016/j.apsusc.2019.05.328
7 S.-W. Lee, S.-H. Cha, K.-J. Choi, B.-H. Kang, J.-S. Lee, S.-W. Kim, J.-S. Kim, H.-M. Jeong, S.-A. Gopalan, and D.-H. Kwon: Sensors **16** (2016) 74. https://doi.org/10.3390/s16010074
8 J. Werner, M. Oehme, M. Schmid, M. Kaschel, A. Schirmer, E. Kasper, and J. Schulze: Appl. Phys. Lett. **98** (2011) 061108. https://doi.org/10.1063/1.3555439
9 Y. Hou, Z. Mei, H. Liang, C. Gu, and X. Du: Appl. Phys. Lett. **105** (2014) 133510. https://doi.org/10.1063/1.4897300
10 J. Yu, C. Shan, X. Huang, X. Zhang, S. Wang, and D. Shen: J. Phys. D: Appl. Phys. **46** (2013) 305105. https://doi.org/10.1088/0022-3727/46/30/305105
11 Z. Liu, T. Yamazaki, Y. Shen, T. Kikuta, N. Nakatani, and Y. Li: Sens. Actuators, B **129** (2008) 666. https://doi.org/10.1016/j.snb.2007.09.055
12 T. Schwebel, M. Fleischer, H. Meixner, and C.-D. Kohl: Sens. Actuators, B **49** (1998) 46. https://doi.org/10.1016/S0925-4005(97)00334-1
13 J. Sheng, E. J. Park, B. Shong, and J.-S. Park: ACS Appl. Mater. Interfaces **9** (2017) 23934. https://doi.org/10.1021/acsami.7b04985
14 M. Fleischer and H. Meixner: Sens. Actuators, B **4** (1991) 437. https://doi.org/10.1016/0925-4005(91)80148-D
15 M. Ogita, N. Saika, Y. Nakanishi, and Y. Hatanaka: Appl. Surf. Sci. **142** (1999) 188. https://doi.org/10.1016/S0169-4332(98)00714-4
16 R. Weiher and R. Ley: J. Appl. Phys. **37** (1966) 299. https://doi.org/10.1063/1.1707830
17 D. Zhang, Z. Liu, C. Li, T. Tang, X. Liu, S. Han, B. Lei, and C. Zhou: Nano Lett. **4** (2004) 1919. https://doi.org/10.1021/nl0489283
18 S. S. Farvid, T. Wang, and P. V. Radovanovic: J. Am. Chem. Soc. **133** (2011) 6711. https://doi.org/10.1021/ja111514u
19 S.-J. Young, C.-C. Yang, and L.-T. Lai: J. Electrochem. Soc. **164** (2016) B3013. https://doi.org/10.1149/2.0051705jes
20 S.-J. Young, Y.-H. Liu, M. N. I. Shiblee, K. Ahmed, L.-T. Lai, L. Nagahara, T. Thundat, T. Yoshida, S. Arya, and H. Furukawa: ACS Appl. Electron. Mater. **2** (2020) 3522. https://doi.org/10.1021/acsaelm.0c00556
21 S.-J. Young and Y.-H. Liu: ECS Sensors Plus **1** (2022) 043602. https://doi.org/10.1149/2754-2726/ac9b71
22 S. Arya, P. Mahajan, S. Mahajan, A. Khosla, R. Datt, V. Gupta, S.-J. Young, and S. K. Oruganti: ECS J. Solid State Sci. Technol. **10** (2021) 023002. https://doi.org/10.1149/2162-8777/abe095
23 S. Han, Z. Zhang, J. Zhang, L. Wang, J. Zheng, H. Zhao, Y. Zhang, M. Jiang, S. Wang, and D. Zhao: Appl. Phys. Lett. **99** (2011). https://doi.org/10.1063/1.3670334
24 T. Rakshit, I. Manna, and S. K. Ray: J. Appl. Phys. **117** (2015). https://doi.org/10.1063/1.4905835
25 H. Mahmoudi Chenari, R. Zamiri, D. Maria Tobaldi, M. Shabani, A. Rebelo, J. S. Kumar, S. Salehizadeh, M. Graça, M. Soares, and J. A. Labrincha: J. Sol-Gel Sci. Technol. **84** (2017) 274. https://doi.org/10.1007/s10971-017-4484-y

26 T.-H. Chang, S.-J. Chang, W.-Y. Weng, C.-J. Chiu, and C.-Y. Wei: IEEE Photonics Technol. Lett. **27** (2015) 2083. https://doi.org/10.1109/LPT.2015.2453317
27 C.-H. Lin, R.-S. Chen, T.-T. Chen, H.-Y. Chen, Y.-F. Chen, K.-H. Chen, and L.-C. Chen: Appl. Phys. Lett. **93** (2008) 112115. https://doi.org/10.1063/1.2987422
28 S. Lany and A. Zunger: Phys. Rev. B. **72** (2005) 035215. https://doi.org/10.1103/PhysRevB.72.035215

About the Authors

Artde Donald Kin-Tak Lam received his B.S. degree in mechanical engineering from National Cheng Kung University (Tainan, Taiwan) in 1987, and his Ph.D. degree in electromechanical and mechanical engineering from National Sun Yat-Sen University (Kaohsiung, Taiwan) in 1993. He is a full professor in the School of Design & Straits College of Engineering of Fujian University of Technology, China. His research areas include MEMS, man–machine interfaces, and sensors.

En-Min Huang received his B.S. degree from National Cheng Kung University, Taiwan (R.O.C.). He is now studying for his direct Ph.D. degree at the Institute of Microelectronics at the same university. His research interests are in thin-film transistors and phototransistors.

Sheng-Po Chang received his B.S. degree in electronic engineering from Southern Taiwan University of Science and Technology, Tainan, Taiwan, in 2004, and his M.S. degree in nanotechnology and microsystems engineering and Ph.D. degree in microelectronics, both from National Cheng Kung University (NCKU), Tainan, in 2006 and 2009, respectively. He is currently an assistant professor with the Department of Microelectronics Engineering, National Kaohsiung University of Science and Technology. His current research interests include II–VI and III–V optoelectronic devices, semiconductor physics, solar cells, and nanotechnology.

Shoou-Jinn Chang received his B.S. degree from National Cheng Kung University (NCKU), Tainan, Taiwan, in 1983, M.S. degree from the State University of New York, Stony Brook, NY, USA, in 1985, and Ph.D. degree from the University of California, Los Angeles, CA, USA, in 1989, all in electrical engineering. From 1989 to 1992, he was a research scientist with Nippon Telegraph and Telephone Basic Research Laboratories, Musashino, Tokyo, Japan. He joined the Department of Electrical Engineering, NCKU, in 1992 as an associate professor and was promoted to full professor in 1998. He served as the Director of the Institute of Microelectronics, NCKU, from August 2008 to July 2011, and the Deputy Director of the Center for Micro/

Nano Science and Technology, NCKU, from February 2006 to January 2011. He is currently the Deputy Director of the Advanced Optoelectronic Technology Center, NCKU. From January to March 1999, he was a Royal Society Visiting Scholar at the University of Wales, Swansea, U.K.; from July 1999 to February 2000, he was a Visiting Scholar at the Research Center for Advanced Science and Technology, University of Tokyo, Tokyo, Japan; from August to September 2001, he was a Visiting Scholar at the Institute of Microstructural Science, National Research Council, Canada; from August to September 2002, he was a Visiting Scholar at the Institute of Physics, Stuttgart University, Stuttgart, Germany; and from July to September 2005, he was a Visiting Scholar with the Faculty of Engineering, Waseda University, Tokyo. He is also an honorary professor at Changchun University of Science and Technology, China. His current research interests include semiconductor physics, optoelectronic devices, and nanotechnology. Dr. Chang received the Outstanding Research Award from the National Science Council, Taiwan, in 2004. He is a Fellow of the Optical Society of America (OSA), the International Society for Optical Engineers (SPIE), and the Institute of Electrical and Electronics Engineers (IEEE).